MODELING SOUTH POLAR COLD TRAP TEMPERATURES ON THE MOON. J.-P. Williams[1], D. A. Paige[1], M. A. Siegler[2,3], and J. Martinez-Camacho[2], [1]Department of Earth, Planetary, and Space Sciences, University of California, Los Angeles, CA, USA, [2]Department of Earth Sciences, Southern Methodist University, Dallas, TX, USA, [3]Planetary Science Institute, Tucson, AZ, USA.

Introduction: The polar regions of the Moon hold significant interest for their potential to harbor water ice and other volatile compounds [1]. Due to the relatively low obliquity of the Moon's spin axis relative to the ecliptic, topographic depressions can result in permanently shadowed regions (PSRs) which receive no direct illumination (e.g. [2,3]). Such PSRs can become cold enough to cold trap volatile compounds on geologic timescales [1,4]. Conversely, high standing areas, such as ridges, can receive direct sunlight for extended periods of time. Such areas are favorable for extended duration surface missions as the illumination is optimal for solar power and thermal stability while providing close proximity to PSRs which are of high scientific value for sampling cold trapped volatiles and in situ resource utilization [5].

The presence of water ice in the polar regions has been confirmed by neutron spectroscopy which has shown hydrogen enrichment at the poles [6,7]. Additionally, infrared absorption features, ultraviolet spectral characteristics, and an increase in reflectance, within PSRs corresponding with cryogenic temperatures suggest surficial water ice frosts [e.g. 8,9,10]. The nature of the ice deposits however has remained challenging to quantify as much about the source, distribution, composition, and relationship between surface and subsurface deposits remains unclear.

Temperature is the fundamental quantity controlling the stability and mobility of ices and understanding the temperature history of the polar regions has been essential for modeling the distribution of potential ice deposits (e.g. [11,12]). Temperatures and illumination conditions observed by the Diviner Lunar Radiometer and the Lunar Reconnaissance Obiter Camera (LROC), respectively, are found to vary substantially with both time of day and season in complicated ways due to slopes and shadows [13,14]. The Diviner temperature observations have provided an unprecedented view into the distribution and temporal variability of polar temperatures [13,15]. However, coverage of the diurnal and seasonal temperatures is not exhaustive and systematic gaps persist presently in the data. Additionally, mission planning and landing site characterization often requires spatial resolutions that exceed that of the highest resolution gridded Diviner polar data products of 240 m pixel^{-1} [16].

To provide a more complete picture of the polar temperatures, we are developing thermal models that can augment the existing Diviner data set. To demonstrate the model we simulate the Diviner observations made during the first day of the LRO nominal mission which began on September, 15th, 2009 when LRO transitioned into a near-circular, 2 h period mapping orbit with an average altitude ~50 km (Fig. 1). These models can provide predicted polar temperatures for future missions. We demonstrate this by modeling the temperatures at the start of the upcoming Korean Pathfinder Lunar Orbiter (KPLO/Danuri) primary mission (Fig. 2).

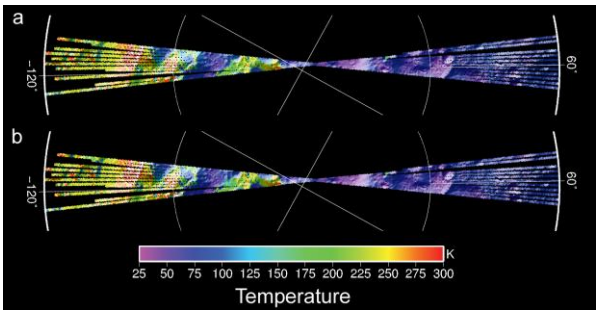

Fig. 1: (a) Bolometric temperatures derived from Diviner observations made on 15-Sept-2009. (b) Modeled temperatures of the observations in (a).

Model: The thermal model accounts for large-scale topographic relief and direct and indirect solar and infrared radiation on the thermal balance of the regolith surface (see [15] for additional details). For the simulations, we used a digital elevation model (DEM) comprised of a ~500-m scale triangular mesh (Fig. 2a) with each triangle coupled to a two-layer regolith thermal model as described in [17]. To compare our model results with Diviner temperatures, we ray-traced each Diviner observation from the first day of the LRO nominal mission onto the same DEM used in the model. Model temperatures were retrieved for each of the corresponding observations. The observed and modeled temperatures were then binned onto a polar stereographic grid for mapping and validating that the model is providing good agreement with the data (Fig. 1). We then simulated the temperatures for January 1st, 2023 which corresponds to the approximate start of the KPLO/Danuri primary mission.

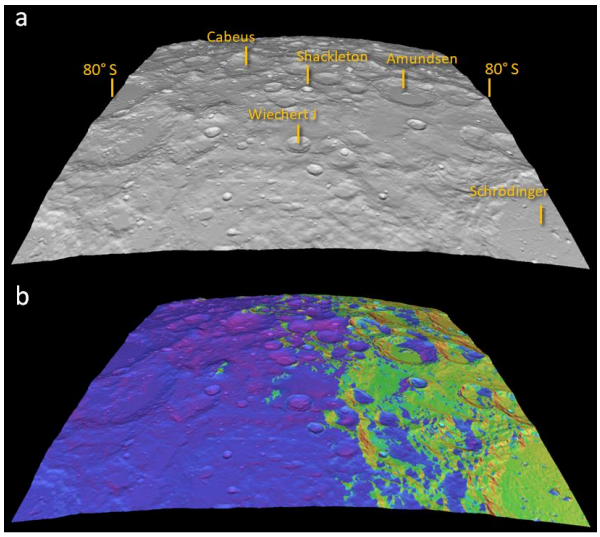

Fig. 2: (a) Shaded relief derived from the DEM used in the thermal model centered on the south pole and extending to 80° S latitude with crater names for reference. (b) The shaded relief colorized by the modeled temperatures predicted to occur on 1-Jan-2023. The temperature color scale is the same as Fig. 1.

Discussion: Fig. 2 shows the estimated temperatures of the south polar region that will be encountered by the KPLO/Daniru mission at the start of its primary mission. The ShadowCam instrument aboard KPLO is designed to image the PSRs at a high resolution and signal-to-noise [18]. Such image capabilities will enable the identification and characterization of albedo patterns and landforms that may be indicative of the presence of ice along with any temporal changes that may suggest accumulation and/or mobilization of volatile deposits and frosts. Our predicted illumination conditions can be compared with observed conditions by ShadowCam. As we continue to modify the model to improve performance and reduce discrepancies with Diviner observations, our model will provide estimates of where and when potential volatile species may be anticipated to accumulate or sublimate throughout the mission. Such predictions can aid in targeting observations and interpreting features observed within images acquired by ShadowCam.

Acknowledgments: The Reduced Data Records data used in this study are publicly available via the Geosciences Node of the Planetary Data System [19].

References: [1] Watson K. et al. (1961) *JGR, 66,* 3033–3045. [2] Bussey D. B. J. et al. (1999) *GRL, 26,* 1187–1199. [3] Mazarico E. (2011) *Icarus, 211,* 1066–1081. [4] Zhang, J. A. & Paige, D. A. (2009) *GRL, 36,* L16203. [5] Neal, C. R. (2020) *LSSW*, #5088. [6] Feldman W. C. et al. (1998) *Science, 281,* 1496–1500. [7] Mitrofanov I. et al. (2012) *JGR, 117,* E00H27. [8] Li S. et al. (2018) *PNAS, 115,* 8907–8912. [9] Hayne P. O. et al. (2015) *Icarus, 255,* 58–69. [10] Fisher E. A. et al. (2017) *Icarus, 292,* 74–85. [11] Siegler M. A. et al. (2015) *Icarus, 255,* 78–87. [12] Schorghofer N & Williams J.-P. (2020) *PSJ, 1,* 54. [13] Williams J.-P. et al. (2019) *JGR, 124,* 2505–2521. [14] Speyerer E. J. & Robinson M. S. (2013) *Icarus, 222,* 122–136. [15] Paige D. A. et al. (2010) *Science, 330,* 479–482. [16] LEAG-MAPSTI Specific Action Team (2021) Final Report of the Lunar Critical Data Products Specific Action Team. [17] Vasavada A. R. et al. (1999) *Icarus, 141,* 179–193. [18] Robinson M. S. et al. (2018) *Lunar Polar Volatiles*, #5028. [19] Paige, D. A. (2010). LRO DLRE LEVEL 4 RDR V1.0, NASA Planetary Data System, LRO-L-DLRE-4-RDR-V1.0. https://doi.org/10.17189/1520651.